

**DESIGN AND DEVELOPMENT OF 200 WATTS  
BIDIRECTIONAL CLLC RESONANT  
CONVERTER FOR UNINTERRUPTIBLE POWER  
SUPPLY APPLICATIONS**

**MUHAMMAD FAIZAL BIN ABDULLAH**

**UNIVERSITI SAINS MALAYSIA**

**2019**

**DESIGN AND DEVELOPMENT OF 200 WATTS BIDIRECTIONAL CLLC  
RESONANT CONVERTER FOR UNINTERRUPTIBLE POWER SUPPLY  
APPLICATIONS**

**by**

**MUHAMMAD FAIZAL BIN ABDULLAH**

**Thesis submitted in fulfilment of the  
requirements for the degree of  
Doctor of Philosophy**

**May 2019**

## ACKNOWLEDGEMENT

I would like to thank my advisor, Associate Professor Ir. Dr. Dahaman Ishak. Till today, I am still amused by his great intuition, broad knowledge and accurate judgment. The most precious thing I learned from him is the attitude toward research, which can be applied to every aspects of life too. Without his guidance and support, I will never be able to achieve this.

I would like to express my deep appreciation to my former supervisor, Prof. Dr. Shahid Iqbal, who introduced me in the area of Power Electronic and kindly gave me guidance and support for my academic research.

I would like to acknowledge the technical support, Mr. Ahmad Shauki Noor, Mr. Jamaluddin Che Amat, Mr. Hairul Nizam Abdul Rahman, Mr. Elias Zainudin and Mr. Amir Hamid for their countless help.

I would like to thank my colleagues, Dr. Nur Azura samsudin, Nurul Asyikin Zawawi, Adrian Tan Soon Theam, Dr. Tiang Tow Liang, Dr Muhammad Imran Shahzad, Muhammad Hafeez Hariri, and Khairul Anuar Norhashim. Their friendships and help have made my research journey pleasant and enjoyable.

My heartfelt appreciation goes toward my father, Abdullah Awang and my mother, Saadah Ishak, who has always encouraged me to give my best. I also want thank my brother, Mohamad Nazir Abdullah, for his help and support.

With deepest love, I would like to thank my wife, Aisy Ameera Raisya Abdullah, who has always been there with her love, support, understanding and encouragement for all my endeavors. Last but not least, I dedicate this dissertation to my son, Ahmad Umair.

## TABLE OF CONTENTS

	<b>Page</b>
<b>ACKNOWLEDGEMENT</b>	ii
<b>TABLE OF CONTENTS</b>	iii
<b>LIST OF TABLES</b>	vi
<b>LIST OF FIGURES</b>	vii
<b>LIST OF ABBREVIATIONS</b>	xiv
<b>LIST OF SYMBOLS</b>	xv
<b>ABSTRAK</b>	xviii
<b>ABSTRACT</b>	xx
<b>CHAPTER ONE : INTRODUCTION</b>	
1.1 Background	1
1.2 Problem statement	4
1.3 Research Objectives	7
1.4 Research Scope	7
1.5 Thesis Outline	8
<b>CHAPTER TWO : LITERATURE REVIEW</b>	
2.1 Introduction	10
2.2 Bidirectional DC-DC Converters	10
2.2.1 Non-isolated Bidirectional DC-DC Converters	11
2.2.2 Isolated Bidirectional DC-DC Converters	13
2.3 Bidirectional Single Phase DC-AC Inverters	26
2.3.1 Switching Technique for Single Phase DC-AC Inverter	27
2.3.1.(a) Sinusoidal Pulse Width Modulation (SPWM) Technique	27
2.3.1.(b) Modified Sinusoidal Pulse Width Modulation (MSPWM) Technique	30
2.3.1.(c) Hybrid Pulse Width Modulation (HPWM) Technique	31
2.3.1.(d) Random Switching HPWM (RS-HPWM) Technique	32

2.3.2	Advanced Bidirectional Single Phase Full-bridge Inverter Topologies	33
2.4	Discussion on the presented Topologies and Techniques	35
2.5	Summary	39
<b>CHAPTER THREE : METHODOLOGY</b>		
3.1	Introduction	41
3.2	Bidirectional CLLC Resonant Converter	43
3.2.1	Topology Description and Modes of Operations	43
3.2.1.(a)	Forward Mode	44
3.2.1.(b)	Backward Mode	45
3.2.2	Analytical Derivation of CLLC Resonant Tank	45
3.2.3	Gain Analysis	48
3.2.4	Analysis and Steady-State Operation of the Converter	54
3.2.4.(a)	Forward Mode	55
3.2.4.(b)	Backward Mode	58
3.3	Bidirectional SPWM Inverters	60
3.3.1	HPWM Inverter	60
3.3.1.(a)	Topology Description and Principle of Operation	61
3.3.1.(b)	Analysis of the Inverter	61
3.3.2	A Highly Efficient Sine-wave Inverter	63
3.3.2.(a)	Topology Description and Principle of Operation	64
3.3.2.(b)	Analysis of the Inverter	66
3.4	Summary	70
<b>CHAPTER FOUR : DESIGN AND IMPLEMENTATION</b>		
4.1	Introduction	72
4.2	Design of Power Stage	72
4.2.1	Forward Mode	75
4.2.2	Backward Mode	80
4.3	Design of CLLC Resonant Tank	83
4.4	Calculation of CLLC Design Parameters and Filter Elements	88

4.5	Charging Procedures During Backward Mode	93
4.6	Calculation of Maximum Voltage and Current Stress	97
4.7	Simulation and Experimental Setup	101
4.8	Hardware Circuitry	103
4.8.1	Main Power Circuit	103
4.8.2	Control Signal Generation Circuit	105
4.8.3	Gate Drive Circuit	106
4.8.4	Sensing Circuit	108
4.9	Design of Transformer	110
4.10	Summary	113
<b>CHAPTER FIVE : RESULTS AND DISCUSSION</b>		
5.1	Introduction	114
5.2	Simulation and Experimental Results for Forward Mode	114
5.3	Simulation and Experimental Results for Backward Mode	134
5.4	Summary	140
<b>CHAPTER SIX : CONCLUSION</b>		
6.1	Conclusion	142
6.2	Recommendation for Future Work	144
<b>REFERENCES</b>		145
<b>APPENDICES</b>		
Appendix A: Derivation of Voltage Gain for CLLC Resonant Tank		
Appendix B: Matlab Command Code For 3-D Plot of Normalized DC Gain		
Appendix C: Matlab Command Code of Normalized DC Gain for Different Quality Factor		
Appendix D: Derivation of Equations for Section 4.2		
Appendix E: Sealed Lead Acid Battery		
Appendix F: PCB Layout and Schematic Diagram		
Appendix G: Arduino Programming Code		
<b>LIST OF PUBLICATIONS</b>		

## LIST OF TABLES

		<b>Page</b>
Table 2.1	Summary of the bidirectional DC-DC converters.	38
Table 2.2	Switching techniques for full-bridge inverter.	39
Table 4.1	Specifications and parameters of the bidirectional UPS.	93
Table 4.2	Key operating points during charging operation.	95
Table 4.3	Equations of voltage and current stress across power switches and other circuit components of the UPSes during forward and backward modes.	97
Table 4.4	Maximum voltage and current stress across power switches and other circuit components of the UPSes during forward and backward modes.	100
Table 4.5	Main power components	103
Table 5.1	Experimental data during forward mode.	134
Table 5.2	Experimental data during backward mode.	140

## LIST OF FIGURES

		<b>Page</b>
Figure 1.1	Simplified diagram of the Offline UPS.	2
Figure 1.2	Simplified diagram of the Ferroresonant UPS.	2
Figure 1.3	Simplified diagram of the Line interactive UPS.	3
Figure 1.4	Simplified diagram of the Online UPS.	4
Figure 1.5	Simplified diagram of UPS. (a) Conventional UPS. (b) Bidirectional UPS.	5
Figure 2.1	Basic structure of bidirectional DC-DC converter.	10
Figure 2.2	Bidirectional buck-boost DC-DC converter [17], [18].	11
Figure 2.3	Bidirectional cuk DC-DC converter [19], [20].	12
Figure 2.4	Bidirectional SEPIC DC-DC converter [21].	12
Figure 2.5	Bidirectional two-phase interleaved buck-boost DC-DC converter [22].	12
Figure 2.6	Bidirectional cascaded buck-boost DC-DC converter [23].	13
Figure 2.7	Bidirectional three-level DC-DC converter [24].	13
Figure 2.8	Isolated bidirectional DC-DC converter based on a current-fed full-bridge and a voltage-fed full-bridge [26].	15
Figure 2.9	Isolated bidirectional DC-DC converter based on a current-fed full-bridge and a voltage-fed full-bridge with RCD snubber [27].	15
Figure 2.10	Isolated bidirectional DC-DC converter based on a current-fed full-bridge and a voltage-fed full-bridge with lossless snubber [28].	16
Figure 2.11	Isolated bidirectional DC-DC converter based on a current-fed full-bridge and a voltage-fed full-bridge with active clamp snubber [29].	16
Figure 2.12	Isolated bidirectional DC-DC converter based on a current-fed full-bridge and a voltage-fed half-bridge with active clamp snubber [32].	17



Figure 2.13	Isolated bidirectional DC-DC converter based on a current-fed half-bridge and a voltage-fed half-bridge [33].	17
Figure 2.14	Isolated bidirectional DC-DC converter based on a current-fed push-pull and a voltage-fed half-bridge [34].	18
Figure 2.15	Isolated bidirectional DC-DC converter based on two voltage-fed full-bridges [35].	18
Figure 2.16	Isolated bidirectional DC-DC converter based on a voltage-fed half-bridge and a voltage-fed full-bridge [39].	19
Figure 2.17	Isolated bidirectional DC-DC converter based on two voltage-fed half-bridges [40].	19
Figure 2.18	Isolated bidirectional DC-DC converter based on two voltage-fed full-bridges with a series resonant network [42].	20
Figure 2.19	DC characteristic of full-bridge series resonant converter.	21
Figure 2.20	DC characteristic of conventional full-bridge LLC resonant converter [54].	24
Figure 2.21	Isolated bidirectional DC-DC converter based on two voltage-fed full-bridges with a LLC resonant tank [55].	24
Figure 2.22	Isolated bidirectional DC-DC converter based on two voltage-fed full-bridges with a LLC resonant tank and an auxiliary inductor [56].	25
Figure 2.23	Isolated bidirectional DC-DC converter based on two voltage-fed full-bridges with a CLLC resonant tank [57].	26
Figure 2.24	Basic structure of bidirectional DC-AC inverter.	26
Figure 2.25	Bidirectional full-bridge inverter topology.	27
Figure 2.26	Key waveform of BPWM.	29
Figure 2.27	Key waveform of UPWM.	30
Figure 2.28	Key waveform of MSPWM technique.	31
Figure 2.29	Key waveform of HPWM technique.	32
Figure 2.30	Key waveform of RS-HPWM technique.	33

Figure 2.31	Advanced bidirectional inverter topologies for nonisolated system. a) Dual-buck inverter with parallel configuration. b) H5 topology. c) Single-buck inverter topology. d) H6 topology.	34
Figure 2.32	Basic sub-topologies for isolated bidirectional DC-DC converter.	36
Figure 3.1	The overall design process flow.	42
Figure 3.2	The proposed bidirectional CLLC resonant converter.	44
Figure 3.3	Fundamental components in CLLC resonant tank.	46
Figure 3.4	Fundamental components in CLLC resonant tank.	47
Figure 3.5	CLLC resonant tank derivation. a) T-network. b) Derived network.	47
Figure 3.6	Equivalent circuits for forward and backward modes. a) Forward mode. b) Backward mode.	49
Figure 3.7	Three-dimensional DC gain contour over normalized frequency under different load conditions. a) Conventional LLC. b) Forward mode CLLC. c) Backward mode CLLC.	51
Figure 3.8	DC gain curves over normalized frequency under different quality factor $Q$ . a) Forward mode CLLC. b) Backward mode CLLC.	53
Figure 3.9	Steady-state waveform of the bidirectional CLLC resonant converter. a) Forward mode. b) Backward mode.	55
Figure 3.10	Circuit operation during <i>Stage 1</i> .	56
Figure 3.11	Circuit operation during <i>Stage 2</i> .	56
Figure 3.12	Circuit operation during <i>Stage 3</i> .	57
Figure 3.13	Circuit operation during <i>Stage 4</i> .	57
Figure 3.14	Circuit operation during <i>Stage 5</i> .	58
Figure 3.15	Circuit operation during <i>Stage 1</i> .	58
Figure 3.16	Circuit operation during <i>Stage 2</i> .	59
Figure 3.17	Circuit operation during <i>Stage 3</i> .	59

Figure 3.18	Circuit operation during <i>Stage 4</i> .	60
Figure 3.19	Circuit operation during <i>Stage 5</i> .	60
Figure 3.20	Key steady-state waveforms of RS-HPWM switching technique.	61
Figure 3.21	The equivalent circuit of HPWM inverter. a) Conventional full-bridge inverter. (b-d) Positive buck converter. (e-g) Negative buck converter.	63
Figure 3.22	The equivalent circuit of highly efficient sine-wave inverter.	64
Figure 3.23	Key steady-state waveforms of highly efficient sine-wave inverter.	66
Figure 3.24	The equivalent circuits for full-bridge inverter. (a) <i>Phase I</i> . (b) <i>Phase II</i> .	67
Figure 3.25	The equivalent circuits for control circuit. (a) <i>Mode I</i> . (b) <i>Mode II</i> .	68
Figure 3.26	The equivalent regions of voltage $V_H$ .	69
Figure 4.1	The proposed UPS systems. (a) UPS 1. (b) UPS 2.	73
Figure 4.2	FHA model of the bidirectional UPS. (a) Forward mode. (b) Backward mode.	74
Figure 4.3	Key steady-state waveforms of the resonant current and capacitor voltage of the resonant tank.	75
Figure 4.4	The effect of $\lambda$ value on DC gain curves. a) Small $\lambda$ . b) Large $\lambda$ .	84
Figure 4.5	DC gain curves under different effective resistive load, $R_x$ . a) Forward mode. b) Backward mode.	85
Figure 4.6	DC gain curves under two modes with various capacitance ratio, $\sigma$ . a) Forward mode. b) Backward mode.	87
Figure 4.7	Charging profile of a 24 V 18 Ah SLA battery.	94
Figure 4.8	Voltage curves with respect to CC and CV operating points.	96
Figure 4.9	Flow chart for one charging cycle of SLA battery.	96
Figure 4.10	Simulation model of CLLC resonant converter. (a) Forward mode. (b) Backward mode.	101

Figure 4.11	Simulation model of HPWM inverter.	101
Figure 4.12	Simulation model of highly efficient sine-wave inverter.	102
Figure 4.13	Experimental setup of the UPS.	102
Figure 4.14	Implemented experimental prototype of UPS 1.	104
Figure 4.15	Implemented experimental prototype of highly efficient sine-wave inverter for UPS 2.	104
Figure 4.16	Control signal generation for UPS 1.	105
Figure 4.17	Control signal generation for UPS 2.	106
Figure 4.18	HCPL-3140 gate drive circuit.	107
Figure 4.19	ACPL-C870 voltage sensor circuit.	109
Figure 4.20	Implemented ACPL-C870 voltage sensor.	109
Figure 4.21	ACS712 current sensor circuit.	110
Figure 4.22	Implemented ACS712 current sensor.	110
Figure 4.23	Measurement illustration using LCR meter.	111
Figure 4.24	The design structure of CLLC transformer.	113
Figure 4.25	Implemented CLLC transformer.	113
Figure 5.1	Operating waveforms of bidirectional CLLC resonant converter for $V_{bat} = 22$ V at 50 W. a & b) Simulation waveforms. c & d) Experimental waveforms.	116
Figure 5.2	Operating waveforms of bidirectional CLLC resonant converter for $V_{bat} = 24$ V at 50 W. a & b) Simulation waveforms. c & d) Experimental waveforms.	117
Figure 5.3	Operating waveforms of bidirectional CLLC resonant converter for $V_{bat} = 26$ V at 50 W. a & b) Simulation waveforms. c & d) Experimental waveforms.	118
Figure 5.4	Operating waveforms of bidirectional CLLC resonant converter for $V_{bat} = 22$ V at 100 W. a & b) Simulation waveforms. c & d) Experimental waveforms.	119

Figure 5.5	Operating waveforms of bidirectional CLLC resonant converter for $V_{bat} = 24$ V at 100 W. a & b) Simulation waveforms. c & d) Experimental waveforms.	120
Figure 5.6	Operating waveforms of bidirectional CLLC resonant converter for $V_{bat} = 26$ V at 100 W. a & b) Simulation waveforms. c & d) Experimental waveforms.	121
Figure 5.7	Operating waveforms of bidirectional CLLC resonant converter for $V_{bat} = 22$ V at 150 W. a & b) Simulation waveforms. c & d) Experimental waveforms.	122
Figure 5.8	Operating waveforms of bidirectional CLLC resonant converter for $V_{bat} = 24$ V at 150 W. a & b) Simulation waveforms. c & d) Experimental waveforms.	123
Figure 5.9	Operating waveforms of bidirectional CLLC resonant converter for $V_{bat} = 26$ V at 150 W. a & b) Simulation waveforms. c & d) Experimental waveforms.	124
Figure 5.10	Operating waveforms of bidirectional CLLC resonant converter for $V_{bat} = 22$ V at 200 W. a & b) Simulation waveforms. c & d) Experimental waveforms.	125
Figure 5.11	Operating waveforms of bidirectional CLLC resonant converter for $V_{bat} = 24$ V at 200 W. a & b) Simulation waveforms. c & d) Experimental waveforms.	126
Figure 5.12	Operating waveforms of bidirectional CLLC resonant converter for $V_{bat} = 26$ V at 200 W. a & b) Simulation waveforms. c & d) Experimental waveforms.	127
Figure 5.13	Switching signals of HPWM inverter. a) Simulation waveforms. b) Experimental waveforms.	128
Figure 5.14	Operating waveforms of HPWM inverter for 50 to 200 W. a - d) Simulation waveforms. e - h) Experimental waveforms.	129
Figure 5.15	Harmonics spectrum of HPWM inverter at maximum power of 200 W. a) THD <sub>v</sub> . b) THD <sub>i</sub> .	130
Figure 5.16	Switching signals of highly efficient sine-wave inverter. a-b) Simulation waveforms. c-d) Experimental waveforms.	131
Figure 5.17	Operating waveforms of highly efficient sine-wave inverter. a-b) Simulation waveforms. c-d) Experimental waveforms.	131

Figure 5.18	Operating waveforms of highly efficient sine-wave inverter for 50 to 200 W. a - d) Simulation waveforms. e - h) Experimental waveforms.	132
Figure 5.19	Harmonics spectrum of highly efficient sine-wave inverter at maximum power of 200 W. a) THD <sub>v</sub> . b) THD <sub>i</sub> .	133
Figure 5.20	Plot of efficiency versus output power for forward mode under different load conditions.	134
Figure 5.21	Operating waveforms of bidirectional CLLC resonant converter. a & b) Simulation waveforms. c & d) Experimental waveforms.	135
Figure 5.22	Operating waveforms of bidirectional CLLC resonant converter at point A. a) Simulation waveforms. b) Experimental waveforms.	137
Figure 5.23	Operating waveforms of bidirectional CLLC resonant converter at point B. a) Simulation waveforms. b) Experimental waveforms.	137
Figure 5.24	Operating waveforms of bidirectional CLLC resonant converter at point C. a) Simulation waveforms. b) Experimental waveforms.	137
Figure 5.25	Operating waveforms of bidirectional CLLC resonant converter at point D. a) Simulation waveforms. b) Experimental waveforms.	138
Figure 5.26	Operating waveforms of bidirectional CLLC resonant converter at point E. a) Simulation waveforms. b) Experimental waveforms.	138
Figure 5.27	Operating waveforms of bidirectional CLLC resonant converter at point F. a) Simulation waveforms. b) Experimental waveforms.	138
Figure 5.28	Experimental charging profile of 24 V 18 Ah SLA battery.	139
Figure 5.29	Graph of efficiency for backward mode under different key operating points.	140

## LIST OF ABBREVIATIONS

AC	Alternating Current
DC	Direct Current
DAB	Dual Active Bridge
EMI	Electromagnetic Interference
FHA	Fundamental Harmonic Approximation
PWM	Pulse Width Modulation
PFM	Pulse Frequency Modulation
BPWM	Bipolar Pulse Width Modulation
UPWM	Unipolar Pulse Width Modulation
HPWM	Hybrid Pulse Width Modulation
SPWM	Sinusoidal Pulse Width Modulation
MSPWM	Modified Sinusoidal Pulse Width Modulation
RS-HPWM	Random Switching Hybrid Pulse Width Modulation
THD	Total Harmonic Distortion
UPS	Uninterruptible Power Supply
ZCS	Zero Current Switching
ZVS	Zero Voltage Switching

## LIST OF SYMBOLS

$S_1 - S_{10}$	Power switches
$S_C$	Control switch
$L_r$	Resonant inductance
$L_m$	Magnetizing inductance
$L_{lkp}$	Primary leakage inductance
$L_{lks}$	Secondary leakage inductance
$L_{xm}$	Transformer's magnetizing inductance
$L_F$	Filter inductor
$L_C$	Current limiting inductor
$C_r$	Resonant capacitor
$C_{r1}$	Primary resonant capacitor
$C_{r2}$	Secondary resonant capacitor
$C_i$	Input capacitor
$C_o$	Output capacitor
$C_{dc}$	DC-link capacitor
$C_{D1} - C_{D2}$	Voltage doubler capacitors
$C_F$	Filter inductor
$C_H$	Holding capacitor
$C_{oss}$	Equivalent parasitic capacitance of bridge switches
$R_{o.ac}$	Equivalent ac-load resistance
$R_x$	Effective resistive load
$R_L$	Load resistor
$V_{ds}$	DC source voltage



$V_{dc}$	DC-link voltage
$V_{bat}$	Battery voltage
$V_{o.rms}$	rms inverter output voltage
$V_{AC.rms}$	rms AC grid voltage
$V_Z$	Breakdown voltage for zener diode
$v_{gs}$	Gate to source voltage
$v_{ds}$	Drain to source voltage
$v_{AC}$	AC grid voltage
$v_{AB}$	Voltage across legs A - B
$v_{CD}$	Voltage across legs C - D
$v_H$	Holding capacitor voltage
$v_m$	Magnetizing voltage
$I_{bat}$	Battery current
$i_M$	Magnetizing current
$i_P$	Primary resonant current
$i_S$	Secondary resonant current
$M$	Voltage gain
$M_{forward}$	Voltage gain of forward mode
$M_{backward}$	Voltage gain of backward mode
$Q$	Quality factor
$Z_o$	Characteristic impedance
$\lambda$	Inductance ratio
$\sigma$	Capacitance ratio
$f_n$	Normalized switching frequency
$f_r$	Resonant frequency

$f_s$	Switching frequency
$f_{si}$	Inverter's switching frequency
$f_p$	Lower resonant frequency
$f_o$	Output frequency
$f_c$	Carrier frequency
$f_{co}$	Cut-off frequency
$n_{Tr}$	Transformer turns ratio
$n_{CLLC}$	CLLC transformer turn ratio
$m_a$	Modulation index
$m_f$	Frequency modulation index
$A_r$	Amplitude of reference signal
$A_c$	Amplitude of carrier signal
$p$	Number of pulses per half cycle
$T_r$	Transformer
$s$	Complex number
$P_o$	rms output power
$t_{dead}$	Dead time between upper and lower switches
$T_S$	Total time for one switching cycle
$N_p$	Number of primary turns
$B_m$	Flux density
$A_N$	Cross sectional area of transformer winding

**REKA BENTUK DAN PEMBANGUNAN PENUKAR SALUN CLLC  
DWIARAH 200 WATTS UNTUK APLIKASI BEKALAN KUASA TANPA  
GANGGUAN**

**ABSTRAK**

Bekalan kuasa tanpa gangguan (UPS) digunakan secara meluas untuk menyediakan kuasa yang boleh dipercayai dalam banyak aplikasi kritikal seperti komputer, pusat data, bilik bedah, dan peralatan telekomunikasi. Sistem UPS pada dasarnya terdiri daripada pengecas bateri, bateri, dan penyongsang. Secara konvensional, dua penukar satu arah (pengecas bateri dan penyongsang) sering dilaksanakan secara berasingan di mana setiap penukar akan memproses kuasa dalam satu arah. Walau bagaimanapun, dalam aplikasi tertentu, konfigurasi ini tidak optimum, oleh itu, penukar dwiarah adalah penyelesaiannya. Dalam UPS, konfigurasi penukar dwiarah membawa kepada pengurangan komponen perkakasan kerana pengecas bateri dan penyongsang boleh dibina dalam satu unit penukar. Dalam disertasi ini, reka bentuk terperinci dan pelaksanaan penukar salun CLLC dwiarah dan penyongsang berkecekapan tinggi baru untuk sistem UPS yang menyediakan aliran kuasa dua hala dibentangkan. Dalam topologi - topologi yang dicadangkan, penyongsang dua peringkat dilaksanakan di mana ia terdiri daripada penukar hadapan iaitu penukar salun CLLC dwiarah. Topologi pertama terdiri daripada penyongsang modulasi lebar denyut hibrid (HPWM) yang digabungkan dengan penukar salun dan dinamakan sebagai UPS 1. Topologi kedua terdiri daripada penyongsang gelombang sinus yang sangat efisien yang digabungkan dengan penukar salun dan dinamakan sebagai UPS 2. Topologi - topologi ini menawarkan beberapa kelebihan seperti prestasi pensuisan yang sangat baik, keupayaan operasi menurun/meningkat, dan kawalan pensuisan yang mudah. Keputusan simulasi dan eksperimen prototaip 200 W

dibentangkan untuk perbandingan, analisa, dan pengesahan. Keputusan yang dibentangkan menunjukkan bahawa penukar salun CLLC mencapai pensuisan voltan sifar (ZVS) untuk suis aktif dan pensuisan arus sifar (ZCS) untuk diod penerus sementara penyongsang menunjukkan bentuk gelombang keluaran yang berkualiti dengan kecekapan keseluruhan yang tinggi. Prestasi kecekapan menunjukkan bahawa UPS-UPS yang dicadangkan mampu menghasilkan kecekapan tinggi dalam mod ke hadapan dan mundur. Bagi UPS 1, kecekapan puncak adalah 88.08% dalam mod ke hadapan dan 92.24% dalam mod mundur. Bagi UPS 2, kecekapan puncak adalah 90.71% dalam mod ke hadapan dan 91.82% dalam mod mundur. Apabila dalam mod ke hadapan, kecekapan UPS 2 sedikit lebih tinggi daripada kecekapan UPS 1, tetapi dalam mod mundur, kecekapan UPS 1 sedikit lebih baik daripada kecekapan UPS 2.

**DESIGN AND DEVELOPMENT OF 200 WATTS BIDIRECTIONAL CLLC  
RESONANT CONVERTER FOR UNINTERRUPTIBLE POWER SUPPLY  
APPLICATIONS**

**ABSTRACT**

Uninterruptible power supply (UPS) is widely employed to provide reliable power in many critical applications such as computers, data centers, surgical rooms, and telecommunication equipment. UPS system essentially consists of a battery charger, battery, and inverter. Conventionally, two unidirectional converters (battery charger and inverter) are often implemented separately where each of the converters will process the power in one direction. However, in certain applications, this configuration is not optimal, hence, a bidirectional converter is the solution. In UPS, a bidirectional converter configuration leads to a reduction in hardware components because battery charger and inverter can be built in one converter unit. In this dissertation, a detailed design and implementation of bidirectional CLLC resonant converter and new high efficient inverter for UPS system that provide bilateral power flow are presented. In the proposed topologies, a two-stage inverter is implemented where it consists of a front-end converter namely bidirectional CLLC resonant converter. The first topology consists of hybrid pulse width modulation (HPWM) inverter combined with the resonant converter and named as UPS 1. The second topology consists of highly efficient sine-wave inverter combined with the resonant converter and named as UPS 2. These topologies offer several advantages such as excellent soft switching performance, buck/boost operation capability, and simple switching control. The simulation and experimental results of 200 W prototypes are presented for comparison, analysis, and validation. The presented results show that the CLLC resonant converter achieves zero voltage switching (ZVS) for active switches

and zero current switching (ZCS) for rectifier diodes, while the inverters show good quality output waveforms with high overall efficiency. The efficiency performance shows that the proposed UPSes were able to produce high efficiency in both forward and backward modes. For UPS 1, the peak efficiency was 88.08 % in forward mode and 92.24 % in backward mode. For UPS 2, the peak efficiency was 90.71 % in forward mode and 91.82 % in backward mode. When in forward mode, the efficiency of UPS 2 was slightly higher than the efficiency of UPS 1, but in backward mode, the efficiency of UPS 1 was slightly better than the efficiency of UPS 2.

# CHAPTER ONE

## INTRODUCTION

### 1.1 Background

With the increasing demand of critical applications such as servers, telecommunication systems, medical equipments, computers, and data centers, Uninterruptible Power Supply (UPS) has been widely used due to the fact of its ability to provide highly reliable power supply during power shortage [1]–[3]. UPS can improve the reliability, efficiency and safety of electronic systems. UPS has been extensively incorporated in the power system of hospital, ship, aircraft, satellite and space station. The growing need for this particular power electronic interface necessitates the research and innovation to develop converters with high power efficiency and high power density owing to the development demand in power supply technologies.

There are four major types of UPSes namely Standby UPS, Ferroresonant UPS, Line interactive UPS, and Online UPS. The Standby UPS or better known as Offline UPS is the most common type encountered on a daily basis. It is usually used in low power applications with power of no more than 2 kVA. It normally routes the input line voltage through surge suppressor, filter and transfer switch before finally being routed to the output of UPS device as shown in Figure 1.1. In the event of power failure, the system will switch over to battery backup power. The benefits of this type lie in its simplicity. The battery only starts supplying power when the main power fails, therefore it has high efficiency, robustness, and low cost.

The Ferroresonant UPS or Hybrid UPS is an extension from former Standby UPS design. The difference from the design standpoint is that the transfer switch that

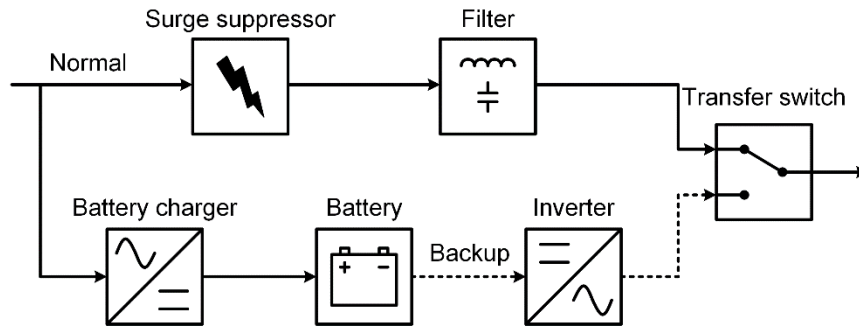


Figure 1.1: Simplified diagram of the Offline UPS [4].

selects between power sources has been replaced by a ferroresonant transformer as shown in Figure 1.2. The transformer has a metal core with two coils of wire wrapped around. When current is applied to one coil, the other coil will magnetically couple to the first coil and induce the current. The transformer consists of three windings with two act as inputs and one as output. The Ferroresonant UPS is usually available in a size range of up to 15 kVA.

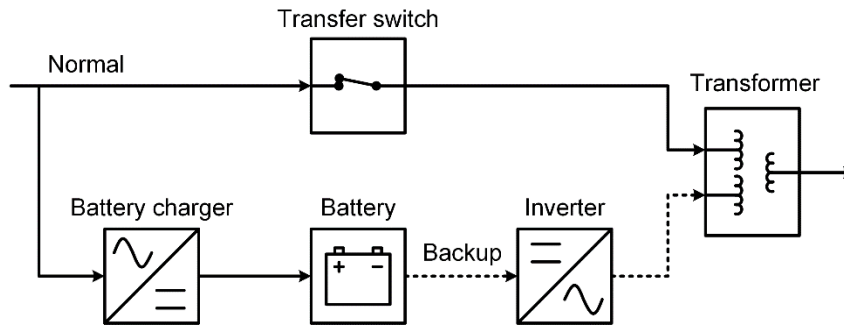


Figure 1.2: Simplified diagram of the Ferroresonant UPS [4].

The Line interactive UPS offers better performance as compared to the previous UPSes and normally served in low and medium power applications of up to 5 kVA. In this UPS, the internal mechanism only consists of an inverter/converter assembly and the transfer switch is located in line with input line voltage as shown in Figure 1.3. During the normal operation, the main power supplies directly to the load while the battery is charged through the inverter/converter. When the main power fails,



the transfer switch opens to disconnect the load from the main line and the backup power will take over and the battery maintains the continuity of power feed to the load through inverter/converter. The main advantage of this type is that the inverter/converter is permanently tied to the output. This allows the amount of times it takes to switch to backup power lesser compared to the previous types.

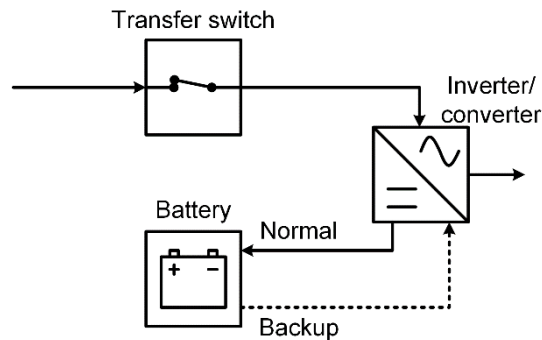


Figure 1.3: Simplified diagram of the Line interactive UPS [4].

The Online UPS has become dominant in high power which is above 10 kVA and high voltage applications in industrial and manufacturing plants. Its internal components are quite similar to the Standby UPS, however the way in which it operates is quite different. During normal condition, the input line voltage is not connected to the output. Instead, the input line voltage is routed to AC-DC converter where the power is used to charge the battery as shown in Figure 1.4. The battery then, discharge its power through inverter and supply power to the output through a transfer switch. The Online UPS will only use the line input power directly when the battery charger, battery or inverter fail. One of the advantage of this type of UPS is total isolation between the input line voltage and output voltage. Compared to the previous types, this UPS does not even require transition times from normal to backup power when main power fails. This allows the system to experience zero interruption when a power failure occurs.

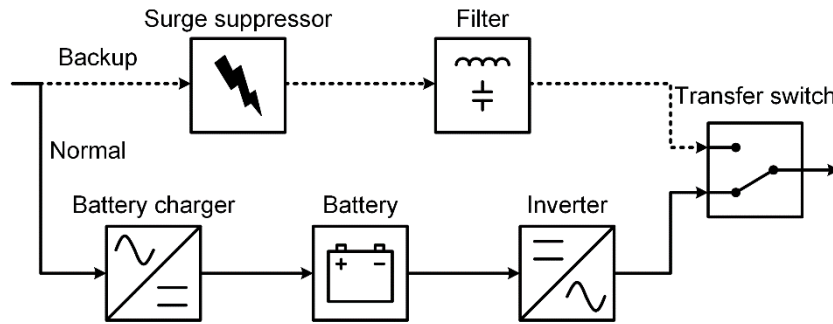


Figure 1.4: Simplified diagram of the Online UPS [4].

Generally, a typical UPS consists a battery charger, a battery bank, and an inverter. Although in some UPS system a single stage DC-AC inverter structure is used, in order to achieve high power efficiency it usually requires two stage structures which consist of DC-DC converter and DC-AC inverter. The two stage architecture which contains front-end DC-DC converter should has high efficiency and high power density performance over wide load condition. As for the DC-AC inverter part, a desirable PWM switching patterns are required in order to achieve lower harmonic contents and lesser ripples in the output waveform.

In this dissertation, a background description and review of the state-of-the-art DC-DC converters and DC-AC inverters are presented. New topologies and control schemes are proposed with the advantages of high efficiency, simple in design and low cost. The detailed design and operation are analyzed and described. A complete two stage architecture is investigated and developed. A simulation and laboratory prototype is tested and implemented and the contributions are discussed and presented in succeeding chapters.

## 1.2 Problem statement

In power electronic application such as UPS, the conversion of power generally requires two steps of exchange which are from main power source to backup power

source and then from backup power source to load when main power is interrupted. In conventional way, two unidirectional converters are often implemented where each of the converters processing the power in one direction [5]. Therefore, multiple converters are used in order to complete the system flow. This reduces the overall system efficiency up to 3 % and increases the cost of system hardware for the additional rectifier circuit that could cost around RM 10. Many conventional UPS designs utilize a separate battery charger and power inversion circuit as shown in Figure 1.5(a). The battery charger or rectifier circuit performs AC-DC inversion and charges the battery while grid power is connected. Whereas, the inverter converts the battery power from DC to AC and supplies to load when grid power fails. One limitation of this conventional topology is that it requires two separate power converters for rectification and charging as well as DC to AC inversion. In addition, the DC-link between inverter and rectifier requires higher voltage level than the battery voltage in order to obtain sufficient DC voltage level for the inverter. Therefore, a number of batteries are required to be connected in series. Hence, for applications that require low power to operate, this configuration is not optimal and economic.

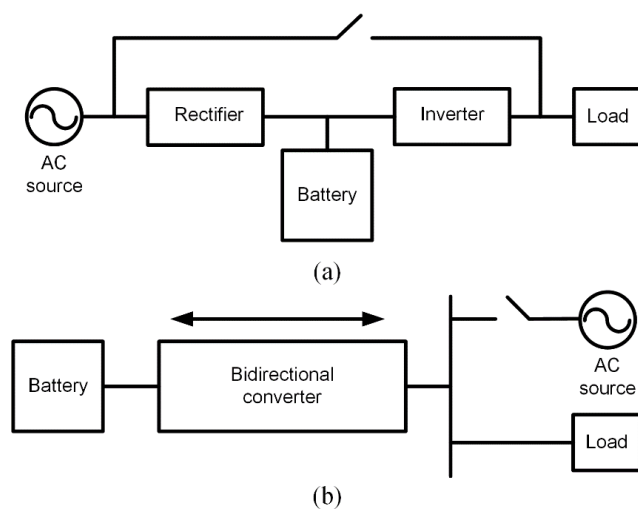


Figure 1.5: Simplified diagram of UPS. (a) Conventional UPS. (b) Bidirectional UPS

[3].

Bidirectional DC-DC converter is an attractive research that has been developed in UPS system recently [6], [7]. Its characteristic feature that capable of bilateral power flow, provides the functionality of two unidirectional converters in a single converter as shown in Figure 1.5(b). Several bidirectional DC-DC converter topologies have been proposed in [6]–[13], focusing on decreasing number of switches, increasing in efficiency and power lost reduction. Bidirectional DC-DC converter topologies can be divided into two types i.e. non-isolated and isolated types. In applications which conversion ratio is not significant and galvanic isolation is not essential, non-isolated types are more preferable due to simplicity in their structure and control scheme. However, isolated types are more convenient for applications that require high voltage conversion ratio as it provides galvanic isolation, thus increases the reliability of the system. There are various isolated bidirectional DC-DC converter topologies which have been proposed in literature such as flyback [14], push-pull [15], dual active bridge, etc. The dual active bridge is the most popular used in isolated bidirectional converter topology [16], [17]. This is because its structure has high efficiency and capability to operate as rectifier or converter depending on the converter's mode. When in forward mode, it operates as converter and when in reverse mode, it operates as bridge rectifier.

In order to improve power density and reduce the size of magnetic component in isolated bidirectional DC-DC converter, high frequency operation is necessary. Unfortunately, high frequency operation exhibits high switching losses in semiconductor devices as was presented in [18] where a single switch that operates at 200 kHz switching frequency with operating voltage of 400 V and current at 4 A is estimated to have 3.46 W of switching losses. Due to this reason, soft switching is desired. Generally, soft switching can be achieved by either zero voltage switching

(ZVS) technique and/or zero current switching (ZCS) technique. In the case of isolated bidirectional DC-DC converter, these two techniques can be realized with snubber, active clamping, resonant switching, parasitic resonance, etc. In isolated unidirectional type UPS, the current topology normally requires around 12 to 18 semiconductor components in one complete system. However, isolated bidirectional type UPS can reduce the number of semiconductor components to only 10. Therefore, this thesis aims to contribute new topologies of isolated bidirectional resonant converter based UPS system. The proposed converters provide a bidirectional power flow control as well as soft switching features that minimize components counts and switching losses.

### **1.3 Research Objectives**

The main aim of this research is to propose a new converter topology for UPS that capable of bilateral power flow. The specific objectives are:

- To design and develop a bidirectional CLLC resonant converter
- To design and develop a highly efficient single phase inverter for UPS system
- To evaluate the performance of the proposed topologies through simulations and experiments

### **1.4 Research Scope**

The main focus of this research is to design and develop a two-stage converter for low power UPS system (< 1kVA) where it consists of two power converters namely bidirectional resonant DC-DC converter and a full-bridge inverter. A brief overview of different topologies for bidirectional DC-DC converter and full-bridge inverter are presented in literature review. Ultimately, research studies on various topologies come to a conclusion with two proposed topology systems for UPS. The topology systems are a new isolated bidirectional CLLC resonant converter with hybrid pulse width

modulation (HPWM) inverter and new isolated bidirectional CLLC resonant converter with a highly efficient sine-wave inverter. Different modes of operation in all stages are explained and the voltage gain of the resonant DC-DC converter is derived. Finally, the feasibility of the proposed converters is verified through computer simulation and experimental testing on laboratory prototypes.

## **1.5 Thesis Outline**

The dissertation consists of six chapters, which are organized as follow.

Chapter 1 gives the detailed introduction of the research background based on general overview of UPS. The efficiency and reliability of bidirectional UPS system design is the main concern. Soft switching techniques and two-stage topologies are the main thesis contributions to improve efficiency and reliability. The research objectives are highlighted and the thesis outline is presented.

Chapter 2 reviews topologies that have been proposed by researchers regarding various bidirectional DC-DC converter topologies as well as various single phase full-bridge inverter topologies. Some latest topologies that have been proposed that related on isolated bidirectional DC-DC converter for UPS are presented. A brief review of basic resonant converter topologies and their DC gain characteristics are presented. The CLLC resonant converter is highlighted in more detail.

Chapter 3 proposes two topology systems for UPS. First, a new isolated bidirectional CLLC resonant converter with HPWM inverter is presented and discussed. An in-depth theory of the proposed bidirectional CLLC resonant converter is presented in detail. A brief topology description of HPWM inverter is presented. Secondly, a new isolated bidirectional CLLC resonant converter with a highly efficient

sine-wave inverter is presented and discussed. An in-depth description of a highly efficient sine-wave inverter is presented.

Chapter 4 discusses the design and implementations of the proposed overall systems. The components selection methods are presented which focus on design procedures for CLLC resonant tank and calculation of maximum voltage and current stress across main power components. Step by step to determine the appropriate values for CLLC resonant tank and filter components are presented. After that, the method for charging the battery is structured from the calculated CLLC resonant tank. Then, implementations for power circuit, control circuit, sensing circuit, and transformer are presented.

Chapter 5 discusses the simulation and experimental results of the proposed topology systems. Experiment measurements collected by using Agilent x1000 are shown to further validate the proposed topology systems. Converter operation constraints are also discussed. This chapter shows the performance evaluation for the proposed topology systems under various operating conditions of input battery voltage and load resistance.

Chapter 6 provides the conclusions of the thesis based on the research works that have been presented in previous chapters. It also makes recommendations for further research on this topic in the future.

## CHAPTER TWO

### LITERATURE REVIEW

#### 2.1 Introduction

In this chapter, a background description and review of the state-of-the-art bidirectional DC-DC converters are discussed and presented. Then, some topologies of single phase inverter and their existing switching techniques are presented. Finally, a review on recent topologies of bidirectional inverter system is featured. A summary is given in order to highlight the advantages and deficiencies of each topology discussed.

#### 2.2 Bidirectional DC-DC Converters

Based on terminology, bidirectional DC-DC converters operate in two modes of operation considering the difference of voltage amplitude on each side of the converter. For further clarification, the generic circuit structure of bidirectional DC-DC converter is illustrated in Figure 2.1. The converter can be characterized as a voltage fed or a current fed depending upon their energy source either voltage source or current source. The bidirectional DC-DC converter can be categorized into buck or boost type based on the placement of their auxiliary energy storage. The buck type is having energy storage placed on the high voltage side, while the boost type is having

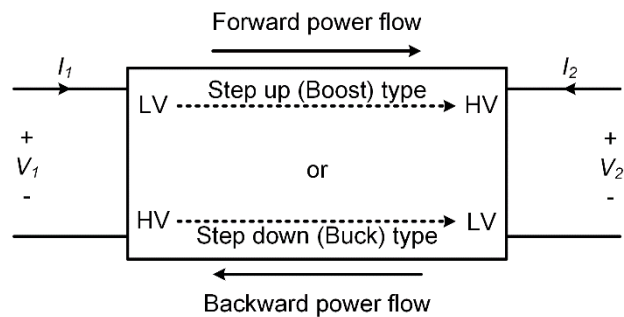


Figure 2.1: Basic structure of bidirectional DC-DC converter [19].



energy storage placed on the low voltage side. In order to realize the bilateral power flow in DC-DC converters, the power switches should be able to carry current on both direction. Therefore, unidirectional semiconductor power switch such as power MOSFET or IGBT in parallel with diode is implemented. So, for buck and boost type converters, the typical switch and diode are replaced by MOSFET/IGBT in parallel with diode. In literature, bidirectional DC-DC converter can be classified into two types which are non-isolated and isolated type. These two are developed based on their own merits in order to meet different application requirements.

### 2.2.1 Non-isolated Bidirectional DC-DC Converters

Non-isolated bidirectional DC-DC converters can be categorized into basic topologies such as buck-boost converter, cuk converter, SEPIC converter and derived topologies such as interleaved buck-boost converter, cascaded buck-boost converter and three level converter. Non-isolated bidirectional DC-DC converters have the advantages of simple structure, low cost, and high reliability. Among these converters, bidirectional buck-boost DC-DC converter shown in Figure 2.2 is the simplest and most widely used [20], [21]. Basically, bidirectional buck-boost DC-DC converter is the combination of a step-up stage and step-down stage connected in anti-parallel. The converter operates in step-down mode by turning off the switch  $S_2$  and turning on switch  $S_1$  with pulse width modulation (PWM) signal. It operates in step-up mode by turning off the switch  $S_1$  and turning on switch  $S_2$  with PWM signal.

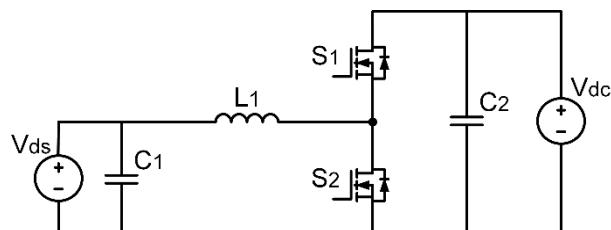


Figure 2.2: Bidirectional buck-boost DC-DC converter [20], [21].

Figure 2.3 shows a bidirectional cuk DC-DC converter [22], [23]. Figure 2.4 shows a bidirectional SEPIC DC-DC converter [24]. Both of these converters are transferring power bidirectionally by using two active switches  $S_1$  and  $S_2$  alternately.

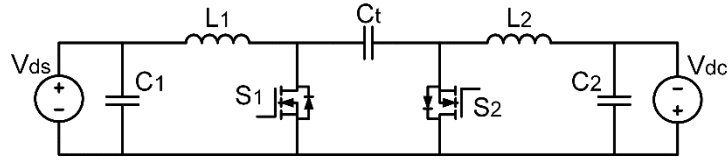


Figure 2.3: Bidirectional cuk DC-DC converter [22], [23].

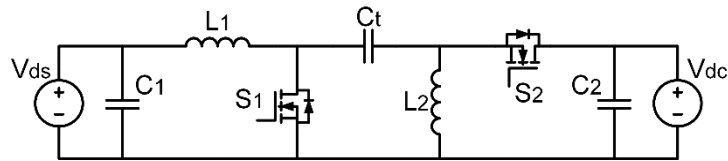


Figure 2.4: Bidirectional SEPIC DC-DC converter [24].

Bidirectional interleaved buck-boost converter is actually a combination of multiple basic bidirectional buck-boost DC-DC converter [25]. Figure 2.5 shows a bidirectional two-phase interleaved buck-boost converter. In this converter, there is  $180^\circ$  phase shift between the gate signal  $S_1$  and  $S_3$  in forward mode, and between the gate signal  $S_2$  and  $S_4$  in reverse mode. The interleaved buck-boost converter is typically used in high current applications. The higher number of interleaving in this converter results in lower output current ripple and smaller inductor can be used for faster dynamic responses.

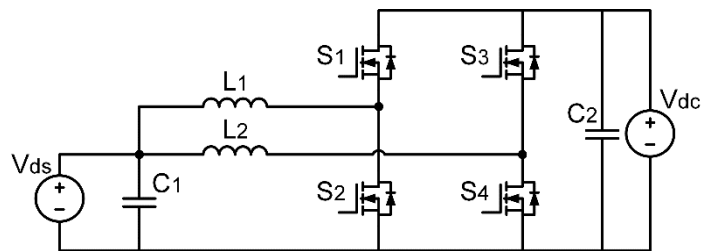


Figure 2.5: Bidirectional two-phase interleaved buck-boost DC-DC converter [25].

Bidirectional cascaded buck-boost converter which is shown in Figure 2.6 is also a derivation from basic bidirectional buck-boost DC-DC converter [26]. The key feature of this converter is that  $V_{ds}$  is not necessarily smaller than  $V_{dc}$ . It is normally used in application where the voltage on one side is either lower or higher than the voltage on the other side.

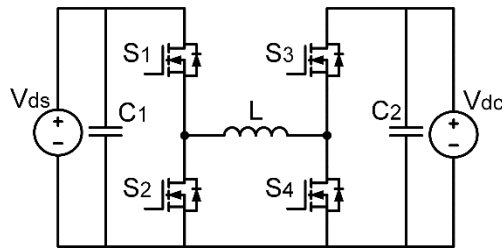


Figure 2.6: Bidirectional cascaded buck-boost DC-DC converter [26].

Another derived bidirectional DC-DC converter is the bidirectional multilevel converters [27]. Figure 2.7 shows an example of bidirectional three-level DC-DC converter. Basically, bidirectional multilevel DC-DC converters are developed for applications that have a high DC-link voltage.

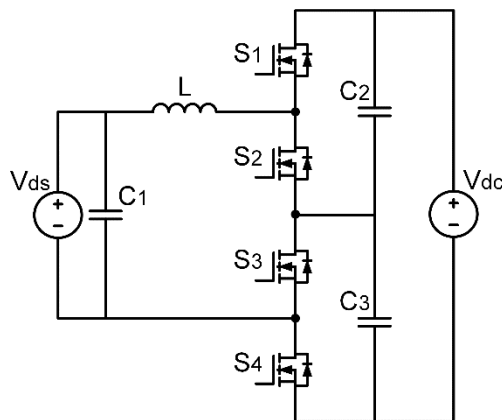


Figure 2.7: Bidirectional three-level DC-DC converter [27].

### 2.2.2 Isolated Bidirectional DC-DC Converters

In the bidirectional DC-DC converters, isolation is generally provided by a transformer. However, transformer basically adds extra size, costs and losses.

Nevertheless, since transformer can provide voltage isolation between two sources and give impedance matching between them, it gives advantages in many applications. The advantages of isolated bidirectional DC-DC converters include galvanic isolation, higher power density, high frequency soft switching with high efficiency, high step-up and step-down voltage ratio and low electromagnetic interference (EMI). Isolated bidirectional DC-DC converters can be divided into two types which are voltage-fed and current-fed. Current-fed isolated bidirectional DC-DC converters normally require switches with much higher voltage rating than the DC input and high voltage stress. Therefore, they are normally suitable for low voltage high current applications [28]. One important characteristic of a voltage-fed isolated bidirectional DC-DC converters is that the output voltage waveform is not affected by the load parameters. The other advantage of voltage-fed isolated bidirectional DC-DC converters is that the voltage sources are commonly available such as battery, DC power supply, or rectified AC bus. Hence, they are easier to be implemented in industrial applications. For the isolated bidirectional DC-DC converters, the sub-topology can be a combination of half-bridge, full-bridge, push-pull and their derivations.

One of the most widely used topologies is the combination of current-fed and voltage-fed full-bridge/ half-bridge/ push-pull and its derivations. Figure 2.8 shows the basic topology structure of this type of converter [29] with a full-bridge structure. The front-end full-bridge is connected to current source or DC inductor, and the other end full-bridge is connected to voltage source or DC capacitor. This topology was proposed for application with low voltage battery and high voltage DC-link. This topology however suffer from several drawbacks due to transformer's non-ideality. This results in leakage inductance and leakage energy stored in the transformer. The

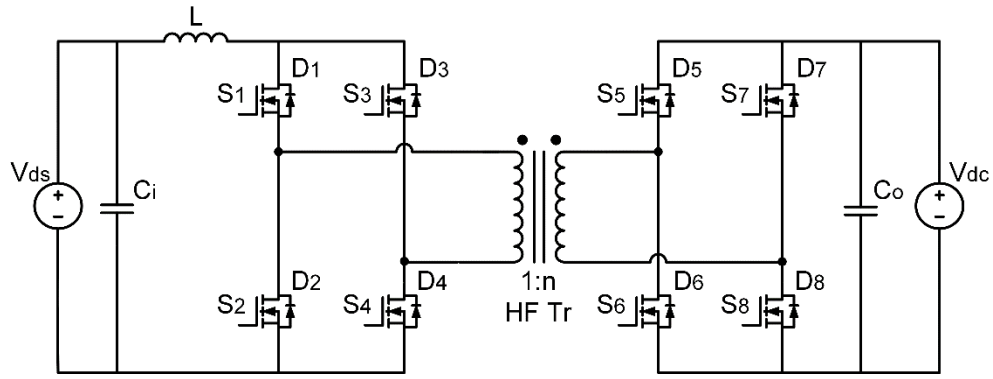


Figure 2.8: Isolated bidirectional DC-DC converter based on a current-fed full-bridge and a voltage-fed full-bridge [29].

leakage energy causes high voltage spikes on switches in current-fed side during switching.

Figure 2.9 shows the improvement made based on earlier topology. A RCD snubber circuit is added into the current-fed side full-bridge to alleviate voltage stress on the switches [30]. A similar approach was employed in [31], to reduce the voltage stress on the switches in current-fed side but lossless snubber was used as shown in Figure 2.10. Based on similar structure, authors in [32]–[34], added an active clamp snubber circuit  $S_c$  and  $C_c$  on the current-fed side full-bridge as shown in Figure 2.11. The addition of active clamp result in ZVS in all switches on current-fed side, and ZVS

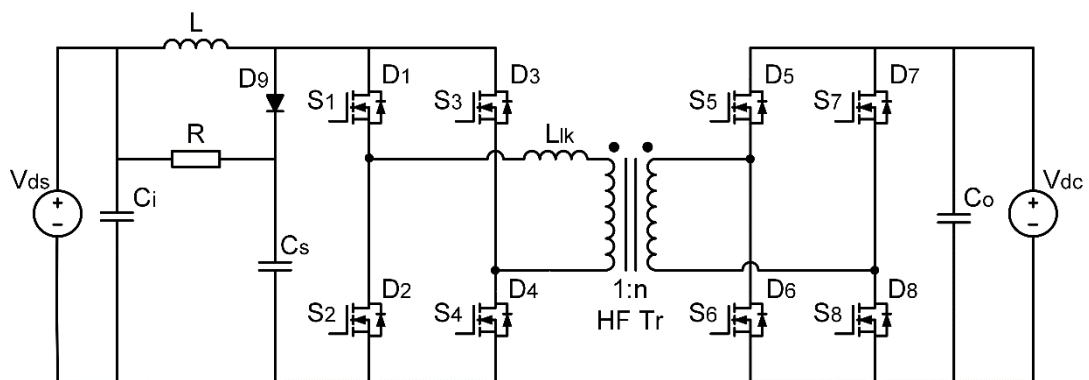


Figure 2.9: Isolated bidirectional DC-DC converter based on a current-fed full-bridge and a voltage-fed full-bridge with RCD snubber [30].

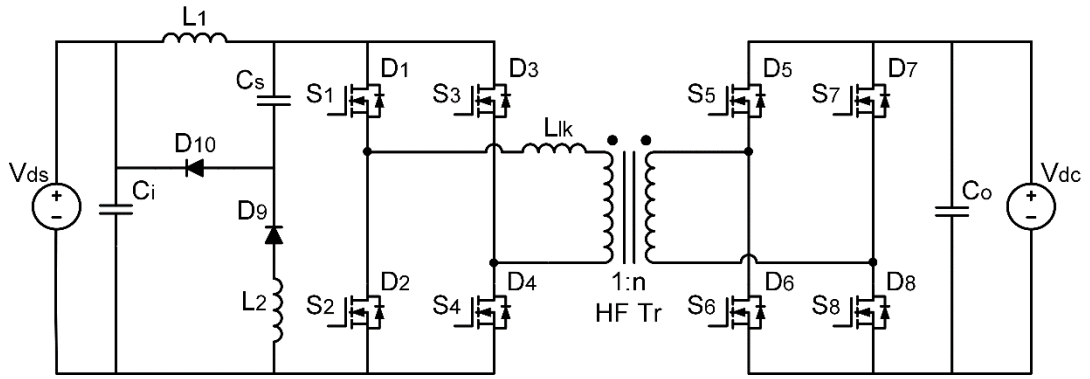


Figure 2.10: Isolated bidirectional DC-DC converter based on a current-fed full-bridge and a voltage-fed full-bridge with lossless snubber [31].

or ZCS achieved in all switches on voltage-fed side. Another derivation of this type of topology was reported in [35], where a half-bridge structure was employed on the voltage-fed side instead of a full-bridge as shown in Figure 2.12. One of the advantages of half-bridge structure is that it can double the voltage when operates as half-bridge rectifier (voltage doubler), thus greatly reduce the number of turns in transformer secondary winding.

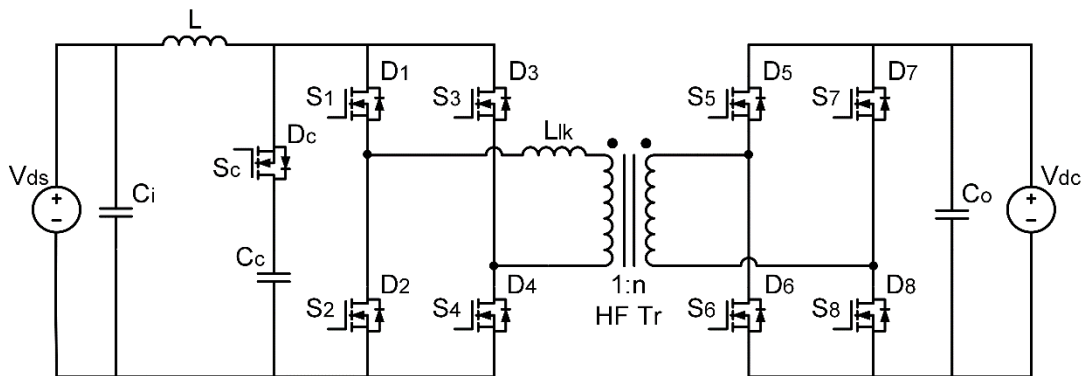


Figure 2.11: Isolated bidirectional DC-DC converter based on a current-fed full-bridge and a voltage-fed full-bridge with active clamp snubber [32].

As shown in Figure 2.13, a half-bridge was employed on both voltage-fed and current-fed side [36]. The advantage of this topology is that it does not require any snubber circuit because  $S_7$  can act as an active clamp switch. Another type of structure

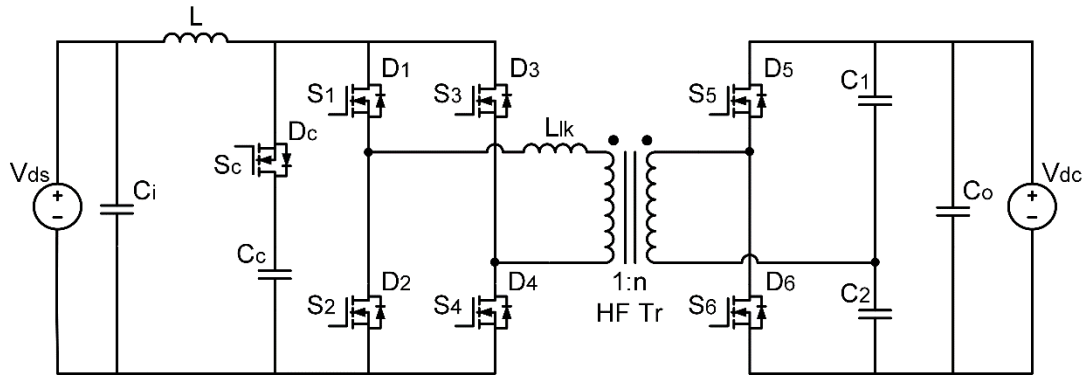


Figure 2.12: Isolated bidirectional DC-DC converter based on a current-fed full-bridge and a voltage-fed half-bridge with active clamp snubber [35].

which does not require any snubber is shown in Figure 2.14 which was reported in [37]. In this topology, a push-pull was employed on current-fed side and half-bridge was employed on voltage-fed side. However, half-bridge topology and push-pull topology require double in input current, resulting double in switch's current stress compared to the full-bridge topology for the same input power. Therefore, these topologies are better for low power applications.

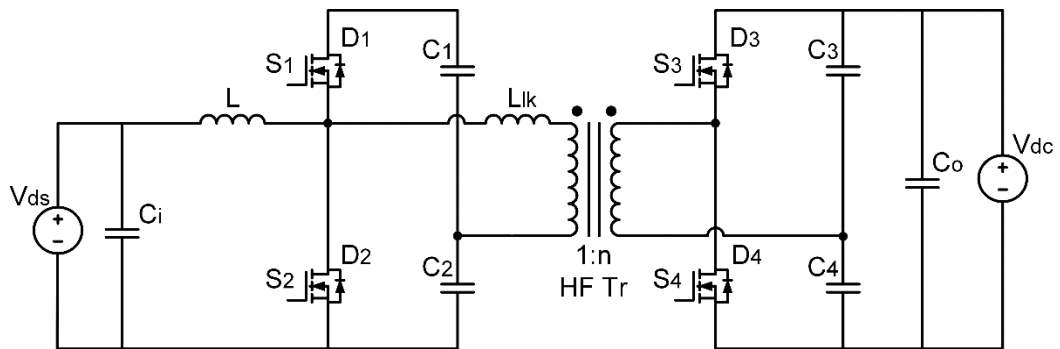


Figure 2.13: Isolated bidirectional DC-DC converter based on a current-fed half-bridge and a voltage-fed half-bridge [36].

The most popular and widely used topology for isolated bidirectional DC-DC converter is dual active bridge (DAB). A typical DAB isolated bidirectional DC-DC converter is shown in Figure 2.15. It utilizes the leakage inductance of the transformer

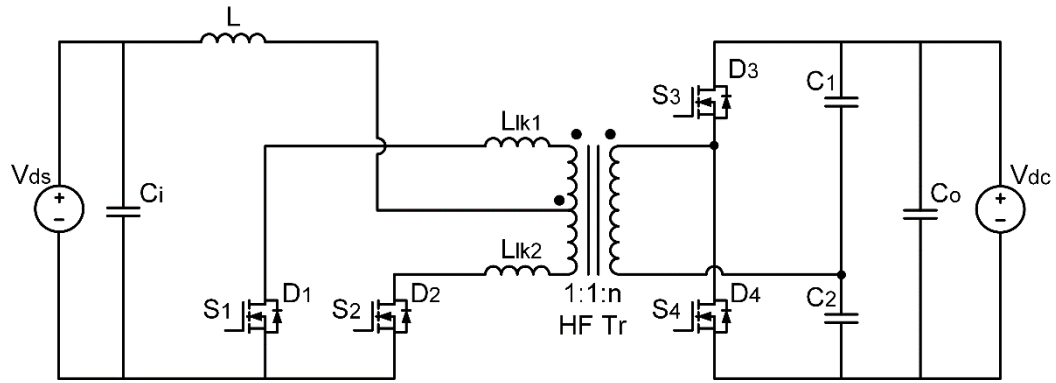


Figure 2.14: Isolated bidirectional DC-DC converter based on a current-fed push-pull and a voltage-fed half-bridge [37].

as the main energy storage and as transfer element to deliver the bidirectional power [38]–[41]. The DAB isolated bidirectional DC-DC converter is a voltage-fed on each side of the isolation transformer. The control of DAB is very simple and straightforward. The control sequence can be either one bridge is phase-shift controlled and the other is uncontrolled (only antiparallel diodes conduct) or both bridges output a square voltage waveforms and the phase between the two voltages square waveform can be controlled. DAB features several advantages such as ZVS can be achieved for switches in both bridges, lower voltage stress on switches compared to current-fed type, and high efficiency.

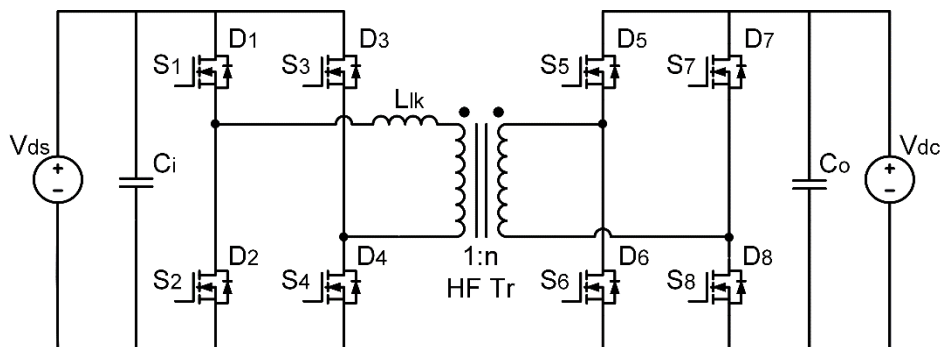


Figure 2.15: Isolated bidirectional DC-DC converter based on two voltage-fed full-bridges [38].



DAB also has few topology derivation, such as the combination of voltage-fed half-bridge and a voltage-fed full-bridge as shown in Figure 2.16 [42], and the combination of two voltage-fed half bridges as shown in Figure 2.17 [43]. This topology however suffers from several drawbacks such as limited voltage range due to limited ZVS range operation, and high turn-off losses. Moreover, at light load conditions, DAB may suffer from hard switching due to energy stored in the leakage inductance may not be large enough to discharge the drain-source capacitances of the switches, thus negating the ZVS feature.

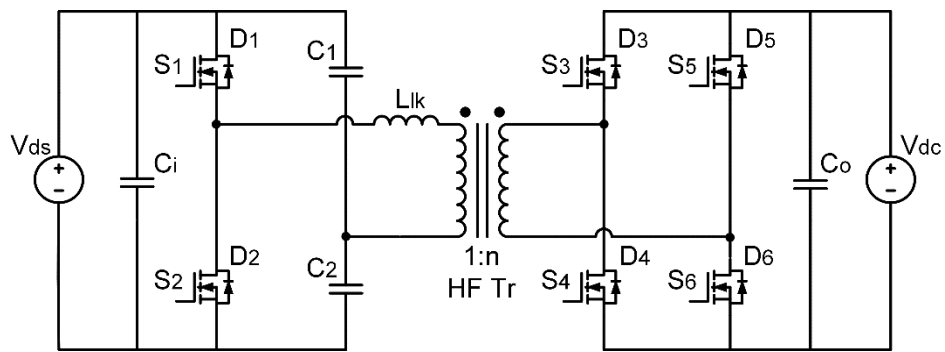


Figure 2.16: Isolated bidirectional DC-DC converter based on a voltage-fed half-bridge and a voltage-fed full-bridge [42].

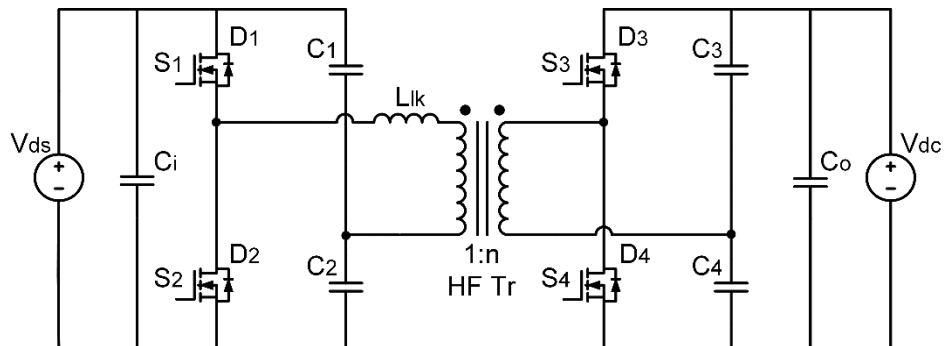


Figure 2.17: Isolated bidirectional DC-DC converter based on two voltage-fed half-bridges [43].

Another popular variant of DAB isolated bidirectional DC-DC converter is bidirectional series resonant DC-DC converter which was reported in [44]–[46] as

shown in Figure 2.18. It consists of two voltage-fed full-bridges and a set of LC resonant tank i.e. capacitor and inductor connected in series. By forming a LC resonant network, a nearly sinusoidal current is obtained which enables low turn-on and turn-off current. Similar to previous design, the control sequence of phase shift angle between the primary and secondary switching-bridges can be employed. Figure 2.19 shows the DC voltage gain characteristic of the series resonant converter where the voltage gain is always less than one. The impedance of the resonant tank changes when the switching frequency changes. The minimum impedance occurs at resonant frequency, so when the switching frequency is equal to resonant frequency, the DC voltage gain of the converter is equal to one. When the switching frequency is above resonant frequency, ZVS is achieved and when the switching frequency is below resonant frequency, ZCS is achieved. The drawback of this converter is wide switching frequency variation range in order to regulate the output voltage especially at light load condition (smaller quality factor,  $Q$ ). Therefore, as the switching frequency drifts away from resonant frequency, the impedance increases, thus more energy circulates in the resonant tank resulting in higher conduction losses. Besides, when it increases the phase shift angles, it produces high turn-off losses and high circulating current.

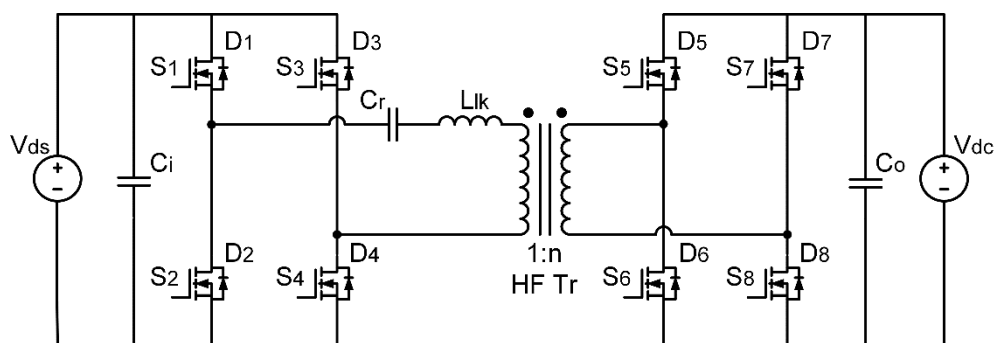


Figure 2.18: Isolated bidirectional DC-DC converter based on two voltage-fed full-bridges with a series resonant network [45].

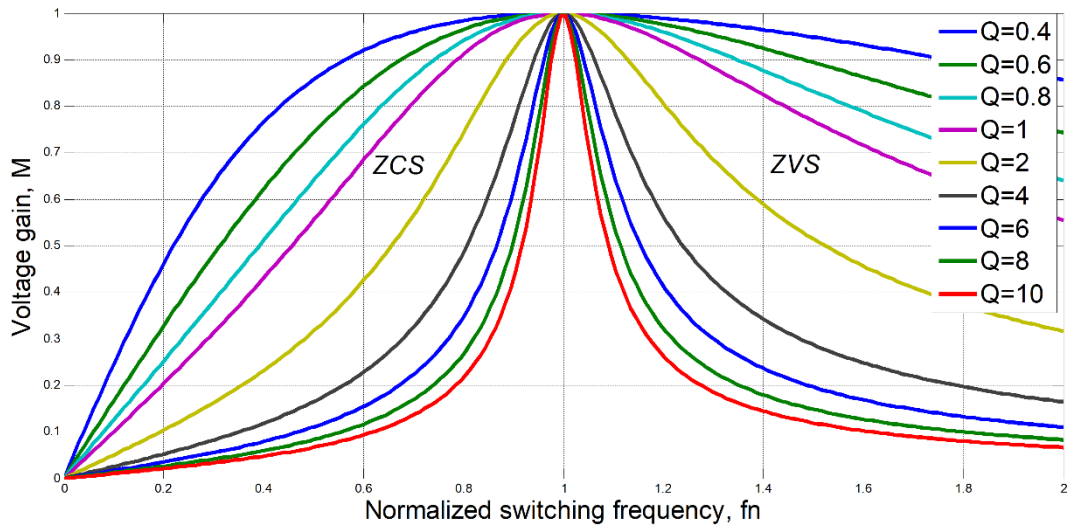


Figure 2.19: DC characteristic of full-bridge series resonant converter [47].

Furthermore, this converter can only operate under buck mode, which is not suitable for wide input and output range applications.

In order to attain wider and higher voltage conversion ratio, improved resonant network with three elements such as LLC resonant network were introduced and among the family of resonant converters, the LLC resonant converter has superiority in performance. This includes buck/boost operation capability, narrow switching frequency variation range and excellent soft switching performance: zero voltage switching (ZVS) of primary active switches and zero current switching (ZCS) of secondary rectifier diodes [48]–[58]. It offers soft switching in all its switches without additional circuitry such as snubber or active clamp. Therefore, a very high frequency switching is possible. Because of this feature, LLC resonant converter is having high efficiency that is always more than 90 %, high power density that is up to 5 kW and smaller hardware components (require only one component for resonant tank).

In the LLC resonant converter, the control sequence only applied to the primary switching-bridge where a fix switching signal with duty ratio of 0.5 is delivered to

bridge's switches. The operation of the bridge switches is similar to the operation of voltage source inverter where the upper switch of one leg is complementary to the lower switch of the other leg of the bridge in which one complementary will be conducting for the first half cycle and the other one will be conducting for the second half cycle. The output voltage regulation of the converter is controlled by the pulse frequency modulation (PFM) technique due to its voltage gain is related with the switching frequency,  $f_s$ . The voltage gain,  $M$  of the conventional LLC resonant converter can be described as follow [48], [49], [51], [52]:

$$M = \frac{1}{\sqrt{(1 + \lambda - \frac{\lambda}{f_n^2})^2 + Q^2(f_n - \frac{1}{f_n})^2}} \quad (2.1)$$

The inductance ratio,  $\lambda$  is defined as below where  $L_r$  is resonant inductance and  $L_m$  is magnetizing inductance:

$$\lambda = \frac{L_r}{L_m} \quad (2.2)$$

The characteristic impedance,  $Z_o$  is defined as below where  $C_r$  is resonant capacitor:

$$Z_o = \sqrt{\frac{L_r}{C_r}} \quad (2.3)$$

The resonant frequency,  $f_r$  of the converter is:

$$f_r = \frac{1}{2\pi\sqrt{L_r.C_r}} \quad (2.4)$$

The lower resonant frequency,  $f_p$  of the converter is:

$$f_p = \frac{1}{2\pi\sqrt{(L_m + L_r).C_r}} \quad (2.5)$$

The normalized switching frequency,  $f_n$  is defined as ratio between switching frequency divided with resonant frequency, where  $f_s$  is the switching frequency:

$$f_n = \frac{f_s}{f_r} \quad (2.6)$$

The quality factor,  $Q$  is defined as below where  $R_{o.ac}$  is the equivalent ac-load resistance and  $n$  is the transformer turns ratio:

$$Q = \frac{Z_o}{n^2 R_{o.ac}} \quad (2.7)$$

As shown in Figure 2.20, the DC voltage gain characteristic of the conventional LLC resonant converter can be divided into three regions [50]. Region I is when the switching frequency,  $f_s$  of the converter is higher than the resonant frequency,  $f_r$ . In this region, the voltage gain is always less than one, and the gain continues to drop as the switching frequency become higher. During operation under this region, the ZVS is achieved on the primary switches. For the Region II, the switching frequency is between two resonant frequencies  $f_p$  and  $f_r$ . In this region, the voltage gain is higher than one and ZVS is achieved on the primary switches. For region III, the ZCS is achievable for the primary switches while ZVS is not achievable. Therefore, for a converter that is controlled with MOSFET, it should be prevented from entering this region.

There are many researches on LLC resonant converter have been reported in the literature [48], [49], [50]– [59]. However, most of them are designed for unidirectional power transfer. In order to realize bidirectional power flow in LLC resonant DC-DC converter, author in [60] proposed isolated bidirectional LLC resonant DC-DC converter as shown in Figure 2.21. This topology is similar to conventional unidirectional LLC converter and having identical performance. However, the converter has lost its LLC feature: ZCS is no longer achieved on the

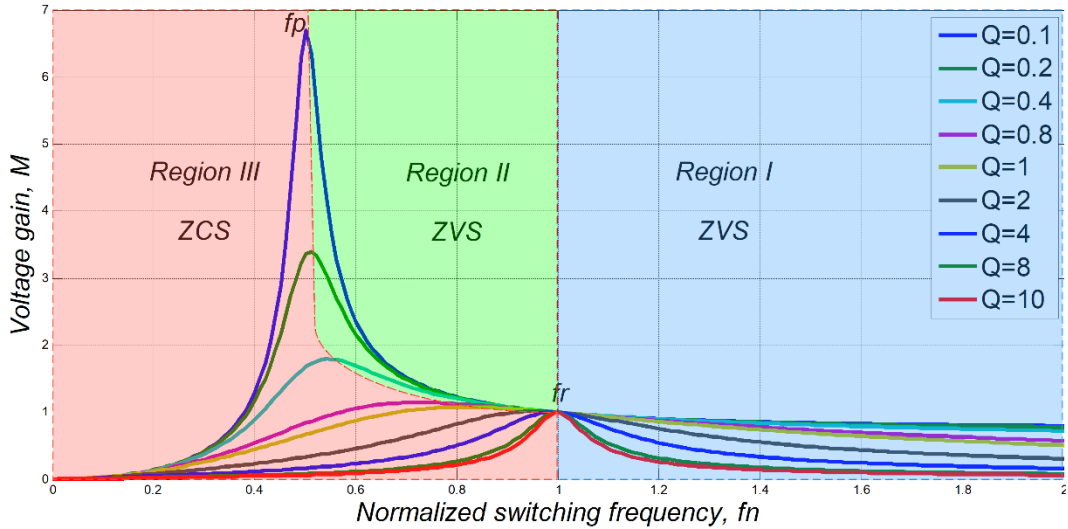


Figure 2.20: DC characteristic of conventional full-bridge LLC resonant converter

[50].

rectifier side when operating in reverse way. Moreover, during the reverse power flow, the magnetizing inductance,  $L_m$  is in parallel with the bridge voltage causing it to no longer participates in resonant network, thus converting the topology into a series resonant DC-DC converter. The efficiency of the converter drops considerably as the switching frequency operates far away from the series resonant frequency, making it unsuitable for wide input and output range applications.

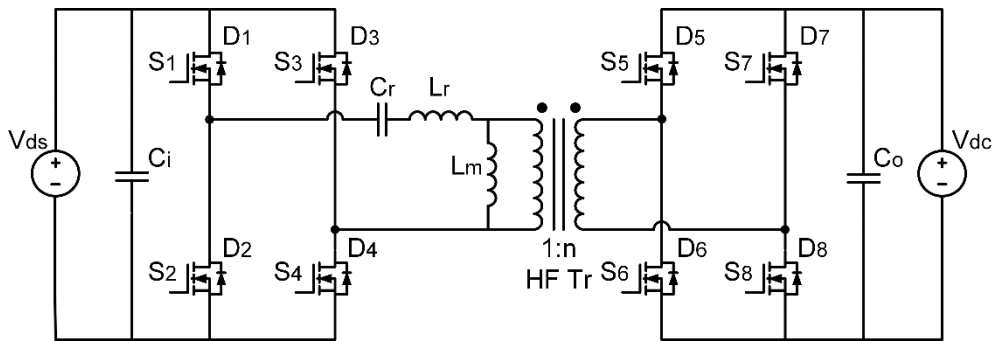


Figure 2.21: Isolated bidirectional DC-DC converter based on two voltage-fed full-bridges with a LLC resonant tank [60].